

NUMERICAL ROCK PHYSICS AND SEISMIC CHARACTERIZATION OF FRACTURED HYDROCARBON RESERVOIRS

Robiel Martínez Corredor^a, Patricia M. Gauzellino^b, Juan E. Santos^{a,c,d} and Rocío S. Hawryszczuk^b

^a*Facultad de Ingeniería, Universidad Nacional de La Plata, Calle 1 y 47, 1900 La Plata, Argentina, robieimatinez@yahoo.com*

^b*Depto de Geofísica Aplicada, Universidad Nacional de La Plata, Paseo del Bosque s/No, 1900 La Plata, Argentina, gauze@fcaglp.unlp.edu.ar*

^c*Conicet, Instituto del Gas y del Petróleo, Facultad de Ingeniería, Universidad de Buenos Aires, Av. Las Heras 2214 Piso 3 C1127AAR Buenos Aires, Argentina*

^d*Department of Mathematics, Purdue University, 150 N. University Street, West Lafayette, Indiana, 47907-2067, USA, santos@math.purdue.edu*

Keywords: Fractures, Anisotropy, Finite Elements, Geophysical Prospecting.

Abstract. In many cases hydrocarbon reservoirs present fractures oriented in preferential directions, which in turn govern fluid flow and reservoir production. This type of reservoirs behaves as anisotropic media in the seismic range of frequencies. In this work we present a collection of finite element harmonic experiments to determine at the macroscale a vertical transversely isotropic viscoelastic equivalent to the hydrocarbon reservoir, which at the mesoscale is described as a fracture fluid-saturated porous medium. Each harmonic experiment is associated with a compressibility or shear test, defined as a boundary value problem with appropriate boundary conditions. The symmetry axis can be changed using an appropriate Bond matrix. This approach allows to represent different scenarios of geophysical interest combining numerical rock physics with wave propagation simulations in the subsurface and wells. In particular, using amplitude versus offset (AVO) simulations, it is possible to infer fracture densities, presence of different fluids and reservoir permeability among others.

1 INTRODUCTION

Naturally fractured reservoirs have received interest in recent years in hydrocarbon exploration geophysics, since, generally, natural fractures control the permeability of the reservoir.

A dense set of horizontal fractures in a fluid-saturated poroelastic medium behaves as a vertically transversely isotropic (VTI) medium when the average fracture distance is much smaller than the predominant wavelength of the traveling waves. This leads to frequency and angular variations of velocity and attenuation of seismic waves. A planar fracture embedded in a fluid saturated poroelastic background medium can be modeled as a extremely thin and compliant porous layer. P-waves traveling in this type of medium induce fluid-pressure gradients at fractures and mesoscopic-scale heterogeneities, generating fluid flow and slow (diffusion) Biot waves, causing attenuation and dispersion of the fast modes (mesoscopic loss). A poroelastic medium with embedded aligned fractures exhibits significant attenuation and dispersion effects due to this mechanism, which can properly be represented at the macroscale with an equivalent VTI medium.

The work by [White et al. \(1975\)](#) was the first to introduce the mesoscopic-loss mechanism in the framework of Biot theory considering porous and thin plane layers. Next, [Gelinsky and Shapiro \(1997\)](#) obtained the relaxed and unrelaxed stiffnesses of the equivalent poroviscoelastic medium to a finely layered horizontally homogeneous material. Later, [Krzikalla and Müller \(2011\)](#) combined the two previous models assuming that fluid flow is perpendicular to the layering plane and independent of the loading direction; they obtained the five complex and frequency-dependent stiffnesses of the equivalent TIV medium.

In this work, we apply a set of compressibility and shear harmonic finite-element (FE) experiments on fractured highly heterogeneous poroelastic samples to determine the five complex and frequency dependent stiffnesses characterizing the equivalent medium.

We also present a brief description of different anisotropic media and the necessary equations to transform an anisotropic symmetry in another, particularly from VTI to HTI (horizontally transversely isotropic) media. Synthetic seismograms are computed by a domain decomposition method combined with a frequency domain FE method. This numerical procedure has already been applied to wave propagation in 2D and 3D media and to different rheological equations.

2 SEISMIC ANISOTROPY

In Seismic, the property of a wave to propagate with a velocity that does not depend on direction is called isotropy. Moreover, elastic media where seismic velocities depend on the direction of wave propagation at some physical points, are called anisotropic. In contrast, a velocity dependence on the spatial location x , is called heterogeneity. It can be said that ordered heterogeneity on microscale results in anisotropy on macroscale.

The anisotropic phenomena are diverse and difficult to classify. Anisotropy is mainly caused by the presence of shales and oriented fractures in the subsurface. It also could be caused by fine layering, but that case usually plays a subsidiary role.

There are different symmetry classes in anisotropic mediums and all of them are described by the stiffness matrix. This matrix is indeed a fourth-rank tensor that relates the displacement tensor and the stress tensor through Hooke's law:

$$\sigma_{ij} = p_{ijkl}e_{kl}, (i, j = 1, 2, 3). \quad (1)$$

It is possible to replace a pair of indexes ij with a single index I , according to Voigt's notation and write Hooke's law in a matrix (as opposed to tensorial) form:

$$\sigma_I = p_{IJ}e_J, (I = 1, \dots, 6). \quad (2)$$

In the present work, transverse isotropy (TI) is used and is the most commonly symmetry used in seismic data processing and velocity-model building. There are several reasons for this: TI is geologically plausible (natural causes are shales and fine layering) and TI media are characterized by relatively few independent stiffness coefficients. Only three combinations of those stiffnesses are needed to describe P-wave traveltimes.

By definition, TI solids have a symmetry axis and are invariants with respect to any rotation around this axis. Therefore it is convenient to describe them in a coordinate frame whose one axis coincides with the axis of rotational symmetry. Media possessing rotational symmetry around the vertical are called vertically transversely isotropic (VTI).

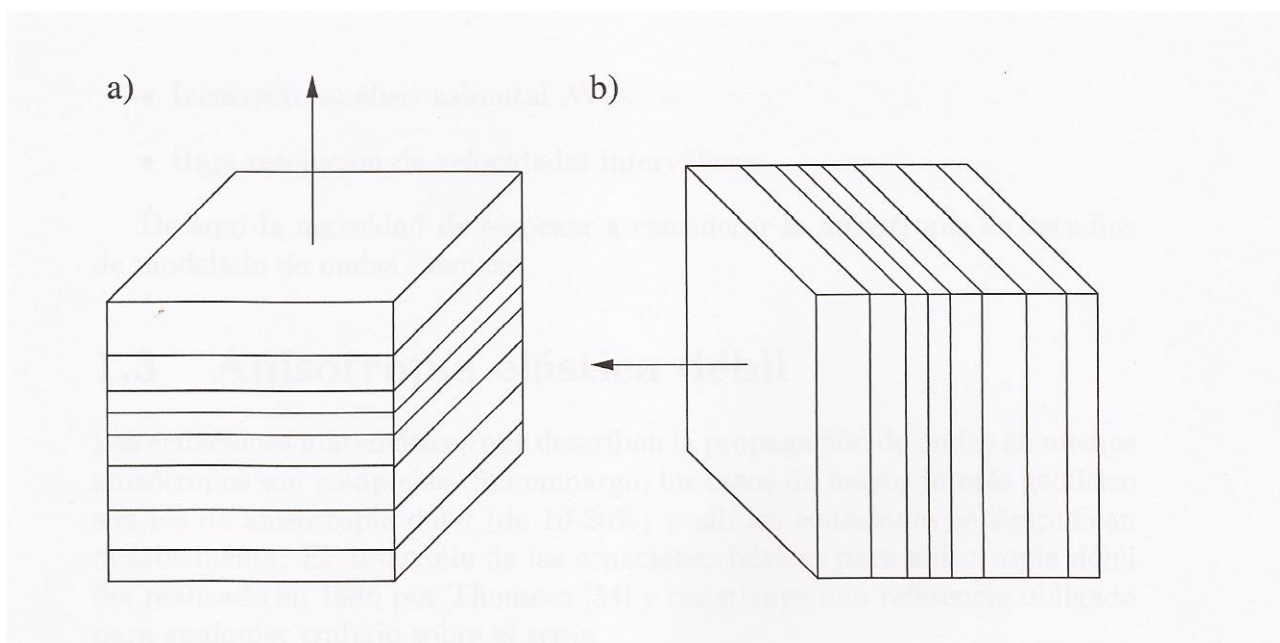


Figure 1: VTI (a), HTI (b)

The VTI stiffness tensor is:

$$\mathbf{P} = \begin{pmatrix} p_{11} & p_{12} & p_{13} & 0 & 0 & 0 \\ p_{12} & p_{11} & p_{13} & 0 & 0 & 0 \\ p_{13} & p_{13} & p_{33} & 0 & 0 & 0 \\ 0 & 0 & 0 & p_{55} & 0 & 0 \\ 0 & 0 & 0 & 0 & p_{55} & 0 \\ 0 & 0 & 0 & 0 & 0 & p_{66} \end{pmatrix} \quad (3)$$

Where:

$$p_{11} = p_{12} + 2p_{66} \quad (4)$$

VTI media (and more generally TI media) are characterized by five independent stiffness coefficients. If the symmetry-axis direction of a TI medium deviates from the vertical, such a medium is called tilted transversely isotropic (TTI). TI media with a horizontal symmetry axis have a special name. They are called horizontally transversely isotropic (HTI). Their significance is in providing the simplest model for anisotropy caused by vertical cracks. In a later section, will be seen that stiffness matrix for an HTI media can be found from a VTI stiffness matrix by performing appropriate rotations of the reference system.(See Fig. 1)

3 THE BIOT MODEL, EQUIVALENT MEDIUM AND SEISMIC PROPERTIES

Let us consider isotropic fluid-saturated poroelastic layers and let $\mathbf{u}^s(\mathbf{x}) = (u_1^s, u_2^s, u_3^s)$ and $\mathbf{u}^f(\mathbf{x}) = (u_1^f, u_2^f, u_3^f)$ indicate the time Fourier transform of the displacement vector of the solid and fluid relative to the solid frame, respectively. Here, if \mathbf{U}^f denotes the fluid displacement vector, $\mathbf{u}^f = \phi(\mathbf{U}^f - \mathbf{u}^s)$, where ϕ is the porosity.

Set $\mathbf{u} = (\mathbf{u}^s, \mathbf{u}^f)$ and let $\boldsymbol{\sigma}(\mathbf{u})$ and $p_f(\mathbf{u})$ denote the time Fourier transform of the total stress and the fluid pressure, respectively, and let $\mathbf{e}(\mathbf{u}^s)$ be the strain tensor of the solid phase. On each plane layer n in a sequence of N layers, the frequency-domain stress-strain relations are [Carcione \(2007\)](#)

$$\sigma_{kl}(\mathbf{u}) = 2\mu e_{kl}(\mathbf{u}^s) + \delta_{kl} (\lambda_G \nabla \cdot \mathbf{u}^s + \alpha M \nabla \cdot \mathbf{u}^f), \quad (5)$$

$$p_f(\mathbf{u}) = -\alpha M \nabla \cdot \mathbf{u}^s - M \nabla \cdot \mathbf{u}^f. \quad (6)$$

The coefficient μ is the shear modulus of the bulk material, considered to be equal to the shear modulus of the dry matrix. The other coefficients in (5)-(6) can be obtained from the relations [Carcione \(2007\)](#)

$$\lambda_G = K_G - \frac{2}{3}\mu, \quad K_G = K_m + \alpha^2 M, \quad (7)$$

$$\alpha = 1 - \frac{K_m}{K_s}, \quad M = \left(\frac{\alpha - \phi}{K_s} + \frac{\phi}{K_f} \right)^{-1},$$

where K_s , K_m and K_f denote the bulk moduli of the solid grains, dry matrix and saturant fluid, respectively.

Denoting by $\omega = 2\pi f$ the angular frequency, Biot's equations of motion in the diffusive range, stated in the space-frequency domain, are

$$\nabla \cdot \boldsymbol{\sigma}(\mathbf{u}) = 0, \quad (8)$$

$$\frac{i\omega\eta}{\kappa} \mathbf{u}^f + \nabla p_f(\mathbf{u}) = 0, \quad (9)$$

where η is the fluid viscosity and κ is the frame permeability.

Let us consider x_1 and x_3 as the horizontal and vertical coordinates, respectively, [Gelinsky and Shapiro \(1997\)](#) showed that the medium behaves as a TI medium with the vertical symmetry axis at long wavelengths. They obtained the relaxed and unrelaxed limits, i.e., the low- and high-frequency limit real-valued stiffnesses, respectively. At all frequencies, the medium behaves as an equivalent VTI medium with complex and frequency-dependent stiffnesses, p_{IJ} , $I, J = 1, \dots, 6$. For the case of flow normal to the fracture layering and independent of the loading direction, these complex stiffnesses can be determined as presented by [Krzikalla and Müller \(2011\)](#) and [Carcione et al. \(2011\)](#).

Denoting by τ the stress tensor of the equivalent VTI medium and by ε the solid strain tensor at the macroscale, the corresponding stress-strain relations, stated in the space-frequency domain, are [Carcione \(1992, 2007\)](#)

$$\tau_{11}(u) = p_{11} \varepsilon_{11}(u^s) + p_{12} \varepsilon_{22}(u^s) + p_{13} \varepsilon_{33}(u^s), \quad (10)$$

$$\tau_{22}(u) = p_{12} \varepsilon_{11}(u^s) + p_{11} \varepsilon_{22}(u^s) + p_{13} \varepsilon_{33}(u^s), \quad (11)$$

$$\tau_{33}(u) = p_{13} \varepsilon_{11}(u^s) + p_{13} \varepsilon_{22}(u^s) + p_{33} \varepsilon_{33}(u^s), \quad (12)$$

$$\tau_{23}(u) = 2 p_{55} \varepsilon_{23}(u^s), \quad (13)$$

$$\tau_{13}(u) = 2 p_{55} \varepsilon_{13}(u^s), \quad (14)$$

$$\tau_{12}(u) = 2 p_{66} \varepsilon_{12}(u^s). \quad (15)$$

Here, we have assumed a closed system, for which the variation of fluid content $\zeta = -\nabla \cdot \mathbf{u}^f$ is equal to zero. This formulation provides the complex velocities of the fast modes at the macroscale and takes into account interlayer flow effects.

The coefficients p_{IJ} in (10)-(15) can be determined by applying five compressibility and shear harmonic FE tests to a representative 2D sample of the fractured poroelastic material. These tests are associated with boundary value problems for Biot's equations (8) stated in the space-frequency domain. The different boundary conditions represent the following virtual experiments [Carcione et al. \(2011\)](#):

1. A compressibility test in the parallel direction to the fracture layering to determine p_{11} .
2. A compressibility test in the normal directions to the fracture layering to determine p_{33} .
3. A test applying simultaneous compressions in both, the normal and parallel directions to the fracture layering to determine p_{13} .
4. A shear test applied in the (x_1, x_3) -plane to determine p_{55} .
5. A shear test in the (x_1, x_2) plane to determine p_{66} .

Regarding the spatial discretization, the computational domain was partitioned uniformly into square cells of side length h .

The FE spaces employed to represent each component of the solid displacement vector \mathbf{u}^s are locally bilinear functions which are globally continuous. The local degrees of freedom (DOF's) are the values of the components of \mathbf{u}^s at the four corners of the computational cells.

On the other hand, the relative fluid displacement \mathbf{u}^f was represented using the vector part of the Raviart-Thomas FE space of zero order [Raviart and Thomas \(1975\)](#). The local DOF's are the values of the normal component of \mathbf{u}^f at the mid points of the faces of the computational cells.

The arguments presented in [Santos et al. \(2009\)](#) can be applied here to show that the error of the FE procedure is of the order of $h^{1/2}$ in the energy norm and of the order h in the L^2 -norm.

For a detailed description of the FE tests used in this work, we refer to [Carcione et al. \(2011\)](#), where the model for these stiffnesses proposed by [Krzikalla and Müller \(2011\)](#) was employed to validate the procedure.

The complex velocities of the equivalent TIV anisotropic medium are [Carcione \(2007\)](#)

$$\begin{aligned} v_{qP} &= (2\bar{\rho})^{-1/2} \sqrt{p_{11}l_1^2 + p_{33}l_3^2 + p_{55} + A}, \\ v_{qSV} &= (2\bar{\rho})^{-1/2} \sqrt{p_{11}l_1^2 + p_{33}l_3^2 + p_{55} - A}, \\ v_{SH} &= \bar{\rho}^{-1/2} \sqrt{p_{66}l_1^2 + p_{55}l_3^2}, \\ A &= \sqrt{[(p_{11} - p_{55})l_1^2 + (p_{55} - p_{33})l_3^2]^2 + 4[(p_{13} + p_{55})l_1l_3]^2}, \end{aligned}$$

where $\bar{\rho} = \langle \rho \rangle$ is the thickness weighted average of the bulk density, $l_1 = \sin \theta$ and $l_3 = \cos \theta$ are the directions cosines, θ is the propagation angle between the wavenumber vector and the x_3 -symmetry axis and the three velocities correspond to the qP, qS and SH waves, respectively. The seismic phase velocity and quality factors are given by

$$v_p = \left[\operatorname{Re} \left(\frac{1}{v} \right) \right]^{-1} \quad \text{and} \quad Q = \frac{\operatorname{Re}(v^2)}{\operatorname{Im}(v^2)}, \quad (16)$$

where v represents either v_{qP} , v_{qSV} or v_{SH} .

The energy-velocity vector \mathbf{v}_e of the qP and qSV waves is

$$\frac{\mathbf{v}_e}{v_p} = (l_1 + l_3 \cot \psi)^{-1} \hat{\mathbf{e}}_1 + (l_1 \tan \psi + l_3)^{-1} \hat{\mathbf{e}}_3, \quad (17)$$

with ψ being the angle between the energy-velocity vector and the x_3 -axis [Carcione \(2007\)](#), while the energy velocity of the SH wave is [Carcione \(2007\)](#)

$$\mathbf{v}_e = \frac{1}{\bar{\rho}v_p} (l_1 p_{66} \hat{\mathbf{e}}_1 + l_3 p_{55} \hat{\mathbf{e}}_3). \quad (18)$$

The FE procedures described above were implemented in FORTRAN language and run in the SUN workstations of the Department of Mathematics at Purdue University. This approach yields the five complex stiffnesses p_{IJ} as a function of frequency and the corresponding phase velocities and dissipation coefficients. For each frequency, the five discrete problems associated with the harmonic compressibility and shear tests were solved using a public domain sparse matrix solver package. This approach yields directly the frequency dependent velocities and dissipation coefficients, instead of solving Biot's equation in the space-time domain and using Fourier transforms to obtain the desired frequency domain characterization at the macroscale.

In all the experiments the numerical samples were discretized using a 160×160 uniform mesh representing 10 periods of 15 cm background sandstone and 1 cm fracture thickness. Both background and fractures have grain density $\rho_s = 2650 \text{ kg/m}^3$, bulk modulus $K_s = 37 \text{ GPa}$ and shear modulus $\mu_s = 44 \text{ GPa}$.

The dry bulk and shear modulus of the samples were determined using the model given by [Krief et al. \(1990\)](#),

$$\frac{K_m}{K_s} = \frac{\mu}{\mu_s} = (1 - \phi)^{3/(1-\phi)}. \quad (19)$$

4 TRANSFORMATION PROPERTIES OF THE STIFFNESS MATRIX IN ANISOTROPIC MEDIA

4.1 Rotation

In the current seismic terminology, a transversely isotropic medium has the symmetry axis along the vertical direction, i.e., the z-axis, as it was presented in expressions (3) and (4).

By performing appropriate rotations of the coordinate system, the medium may become azimuthally anisotropic. The displacement vector u_i and the strain and stress tensor ϵ_{ij} , σ_{ij} must be transform too.

If the transformation matrix is:

$$\mathbf{A} = \begin{pmatrix} a_{11} & a_{12} & a_{13} \\ a_{21} & a_{22} & a_{23} \\ a_{31} & a_{32} & a_{33} \end{pmatrix}, \quad (20)$$

the new tensors will be:

$$\epsilon' = \mathbf{N}\epsilon$$

$$\sigma' = \mathbf{M}\sigma$$

where M and N are called Bond matrices and have the form:

$$\mathbf{N} = \begin{pmatrix} a_{11}^2 & a_{12}^2 & a_{13}^2 & a_{12} a_{13} & a_{13} a_{11} & a_{11} a_{12} \\ a_{21}^2 & a_{22}^2 & a_{23}^2 & a_{22} a_{23} & a_{23} a_{21} & a_{21} a_{22} \\ a_{31}^2 & a_{32}^2 & a_{33}^2 & a_{32} a_{33} & a_{33} a_{31} & a_{31} a_{32} \\ 2 a_{21} a_{31} & 2 a_{22} a_{32} & 2 a_{23} a_{33} & a_{22} a_{33} + a_{23} a_{32} & a_{21} a_{33} + a_{23} a_{31} & a_{22} a_{31} + a_{21} a_{32} \\ 2 a_{31} a_{11} & 2 a_{32} a_{12} & 2 a_{33} a_{13} & a_{12} a_{33} + a_{13} a_{32} & a_{13} a_{31} + a_{11} a_{33} & a_{11} a_{32} + a_{12} a_{31} \\ 2 a_{11} a_{21} & 2 a_{12} a_{22} & 2 a_{13} a_{23} & a_{12} a_{23} + a_{13} a_{22} & a_{13} a_{21} + a_{11} a_{23} & a_{11} a_{22} + a_{12} a_{21} \end{pmatrix}, \quad (21)$$

$$\mathbf{M} = \begin{pmatrix} a_{11}^2 & a_{12}^2 & a_{13}^2 & 2 a_{12} a_{13} & 2 a_{13} a_{11} & 2 a_{11} a_{12} \\ a_{21}^2 & a_{22}^2 & a_{23}^2 & 2 a_{22} a_{23} & 2 a_{23} a_{21} & 2 a_{21} a_{22} \\ a_{31}^2 & a_{32}^2 & a_{33}^2 & 2 a_{32} a_{33} & 2 a_{33} a_{31} & 2 a_{31} a_{32} \\ a_{21} a_{31} & a_{22} a_{32} & a_{23} a_{33} & a_{22} a_{33} + a_{23} a_{32} & a_{21} a_{33} + a_{23} a_{31} & a_{22} a_{31} + a_{21} a_{32} \\ a_{31} a_{11} & a_{32} a_{12} & a_{33} a_{13} & a_{12} a_{33} + a_{13} a_{32} & a_{13} a_{31} + a_{11} a_{33} & a_{11} a_{32} + a_{12} a_{31} \\ a_{11} a_{21} & a_{12} a_{22} & a_{13} a_{23} & a_{12} a_{23} + a_{13} a_{22} & a_{13} a_{21} + a_{11} a_{23} & a_{11} a_{22} + a_{12} a_{21} \end{pmatrix}. \quad (22)$$

If P is the stiffness matrix in the original system, after the rotation it results:

$$\mathbf{P}' = \mathbf{M} \cdot \mathbf{P} \cdot \mathbf{M}^T, \quad (23)$$

where M^T is the transposed matrix of M.

For instance, by doing a rotation of an angle ψ about the y-axis:

$$\mathbf{A} = \begin{pmatrix} \cos \psi & 0 & -\sin \psi \\ 0 & 1 & 0 \\ \sin \psi & 0 & \cos \psi \end{pmatrix} \quad (24)$$

and:

$$\mathbf{M} = \begin{pmatrix} \cos^2 \psi & 0 & \sin^2 \psi & 0 & -\sin(2\psi) & 0 \\ 0 & 1 & 0 & 0 & 0 & 0 \\ \sin^2 \psi & 0 & \cos^2 \psi & 0 & \sin(2\psi) & 0 \\ 0 & 0 & 0 & \cos \psi & 0 & \sin \psi \\ \frac{1}{2} \sin(2\psi) & 0 & -\frac{1}{2} \sin(2\psi) & 0 & \cos(2\psi) & 0 \\ 0 & 0 & 0 & -\sin \psi & 0 & \cos \psi \end{pmatrix}. \quad (25)$$

By using the previous results, an HTI medium can be found through a clockwise rotation by $\pi/2$ about the y-axis,

$$\mathbf{A} = \begin{pmatrix} 0 & 0 & -1 \\ 0 & 1 & 0 \\ 1 & 0 & 0 \end{pmatrix}, \quad (26)$$

$$\mathbf{M} = \begin{pmatrix} 0 & 0 & 1 & 0 & 0 & 0 \\ 0 & 1 & 0 & 0 & 0 & 0 \\ 1 & 0 & 0 & 0 & 0 & 0 \\ 0 & 0 & 0 & 0 & 0 & 1 \\ 0 & 0 & 0 & 0 & -1 & 0 \\ 0 & 0 & 0 & -1 & 0 & 0 \end{pmatrix}, \quad (27)$$

and:

$$\mathbf{P}' = \begin{pmatrix} p_{33} & p_{13} & p_{13} & 0 & 0 & 0 \\ p_{13} & p_{11} & p_{12} & 0 & 0 & 0 \\ p_{13} & p_{12} & p_{11} & 0 & 0 & 0 \\ 0 & 0 & 0 & p_{66} & 0 & 0 \\ 0 & 0 & 0 & 0 & p_{55} & 0 \\ 0 & 0 & 0 & 0 & 0 & p_{55} \end{pmatrix}. \quad (28)$$

4.2 Azimuthal anisotropy

By making appropriate rotations of the coordinate system, the medium may become azimuthally anisotropic. An example is a transversely isotropic medium whose symmetry axis is horizontal and makes an angle θ with the x-axis. To obtain this medium, we perform a clockwise rotation by $\pi/2$ about the Y-axis:

$$\mathbf{A} = \begin{pmatrix} 0 & 0 & -1 \\ 0 & 1 & 0 \\ 1 & 0 & 0 \end{pmatrix} \quad (29)$$

followed by a counterclockwise rotation by θ about the new Z-axis:

$$\mathbf{B} = \begin{pmatrix} \cos \theta & -\sin \theta & 0 \\ \sin \theta & \cos \theta & 0 \\ 0 & 0 & 1 \end{pmatrix}. \quad (30)$$

The corresponding total rotation matrix is given by:

$$\mathbf{ROT} = \mathbf{A} \mathbf{B}. \quad (31)$$

The associated Bond transformation matrix is:

$$\mathbf{M} = \begin{pmatrix} 0 & \sin^2 \theta & \cos^2 \theta & \sin(2\theta) & 0 & 0 \\ 0 & \cos^2 \theta & \sin^2 \theta & -\sin(2\theta) & 0 & 0 \\ 1 & 0 & 0 & 0 & 0 & 0 \\ 0 & 0 & 0 & 0 & -\sin \theta & \cos \theta \\ 0 & 0 & 0 & 0 & -\cos \theta & -\sin \theta \\ 0 & -\frac{1}{2} \sin(2\theta) & \frac{1}{2} \sin(2\theta) & -\cos(2\theta) & 0 & 0 \end{pmatrix}, \quad (32)$$

and therefore the new stiffness coefficients can be found with this matrix.

5 THE SEISMIC MODELING METHOD

The algorithm used to simulate the wavefields is the FE method in the space-frequency domain, where the frequency-dependent anelastic effects can be described exactly without approximations [Carcione et al. \(2006\)](#); [Carcione \(2007\)](#). Let us consider a 2D volume of an anisotropic and viscoelastic medium, $\Omega = [0, 1]^2$, with boundary $\Gamma = \partial\Omega$. Let $u(x, \omega)$ denote the displacement vector at the angular frequency ω . We work with an *HTI* media which is obtained by applying a rotation as described in section 4.

The equation governing the motion is

$$-\rho(x)\omega^2 u(x, \omega) - \nabla \cdot \sigma[u(x, \omega)] = f(x, \omega), \quad x \in \Omega, \quad (33)$$

with absorbing boundary conditions

$$-\sigma[u(x, \omega)] \cdot \nu = i\omega\sqrt{\rho}D^{1/2}u(x, \omega), \quad x \in \Gamma, \tag{34}$$

where

$$D = \begin{pmatrix} p_{11}\nu_1^2 + p_{55}\nu_3^2 & 2(p_{15}\nu_1^2 + p_{35}\nu_3^2) \\ 2(p_{15}\nu_1^2 + p_{35}\nu_3^2) & p_{55}\nu_1^2 + p_{33}\nu_3^2 \end{pmatrix}. \tag{35}$$

In equation (33), σ and f represent the stress tensor and the external-source vector, respectively. The boundary Γ is transparent for normally incident waves and ν denotes the unit outward vector normal on Γ . The derivation can be found in Love (1994) and Lovera and Santos (1988).

We proceed to formulate the variational form of (33)-(34): Find $u(x, \omega) \in [H^1(\Omega)]^2$ such that

$$-(\rho\omega^2u, \varphi) + (\sigma(u), \varepsilon(\varphi)) + i\omega \langle \sqrt{\rho}D^{1/2}u, \varphi \rangle_\Gamma = (f, \varphi), \quad \varphi \in [H^1(\Omega)]^2, \tag{36}$$

where ε is the strain tensor. Here $(f, g) = \int_\Omega fg^* dx$ and $\langle f, g^* \rangle = \int_\Gamma fg^* d\Gamma$ indicate the complex $[L^2(\Omega)]^2$ and $[L^2(\Gamma)]^2$ inner products, where “*” denotes complex conjugate. $H^1(\Omega)$ denotes the usual Sobolev space of function in $L^2(\Omega)$ with first derivatives in $L^2(\Omega)$. The arguments given in Ha et al. (2002) and Douglas et al. (1994) can be used to show that existence and uniqueness holds for the solution of (36).

Numerical dispersion is an important aspect to be taken into account when using wave propagation algorithms. It is shown in Zyserman et al. (2003) that using the nonconforming FE space \mathcal{NC}^h described in Douglas et al. (1995) allows to use about half the number of points per wavelength to achieve a desired tolerance in numerical dispersion as compared with standard conforming bilinear elements. Thus, we will employ the FE space \mathcal{NC}^h described below to compute an approximate solution of (36).

Let τ^h be a quasi-regular partition of $\bar{\Omega}$ such that $\bar{\Omega} = \cup_{j=1}^J \Omega_j$ with Ω_j being rectangles of diameter bounded by h . Set $\Gamma_j = \partial\Omega \cap \partial\Omega_j$ and $\Gamma_{jk} = \Gamma_{kj} = \partial\Omega_j \cap \partial\Omega_k$; we denote by ξ_j and ξ_{jk} the centroids of Γ_j and Γ_{jk} , respectively. Consider the reference rectangular element

$$R = [-1, 1]^2, \quad S(R) = \text{Span} \left\{ 1, x, z, \left(x^2 - \frac{5}{3}x^4 \right) - \left(z^2 - \frac{5}{3}z^4 \right) \right\}.$$

The degrees of freedom associated with S are the values at the mid points of the faces of R .

For example, if $a_1 = (-1, 0)$, $a_2 = (0, -1)$, $a_3 = (1, 0)$ and $a_4 = (0, 1)$, the basis function $\psi_1(x, z) = \frac{1}{4} - \frac{1}{2}x - \frac{3}{8} \left[\left(x^2 - \frac{5}{3}x^4 \right) - \left(z^2 - \frac{5}{3}z^4 \right) \right]$ is such that $\psi_1(a_1) = 1$ and $\psi_1(a_j) = 0$, $j = 2, 3, 4$.

Then,

$$\mathcal{NC}^h = \{ \varphi \in [L^2(\Omega)]^2 : \varphi_j \in [S(\Omega_j)]^2, \quad \varphi_j(\xi_{jk}) = \varphi_k(\xi_{jk}) \forall j, k \},$$

where φ_j denotes the restriction of φ as seen from Ω_j . Now the global nonconforming approximation u^h to the solution u of (36) can be stated as follows: Find $u^h \in \mathcal{NC}^h$ such that

$$-(\rho\omega^2u^h, \varphi) + \sum_j (\sigma(u^h), \varepsilon(\varphi))_{\Omega_j} + i\omega \langle \sqrt{\rho}D^{1/2}u^h, \varphi \rangle_\Gamma = (f, \varphi), \quad \varphi \in \mathcal{NC}^h. \tag{37}$$

It can be shown (see Ha et al. (2002) for the isotropic case) that for h sufficiently small the error associated with the global procedure (37) is of order h^2 in the L^2 -norm and of order h in the broken H^1 -energy norm.

Note that (37) is a noncoercive elliptic Helmholtz-type problem, so that the usual iterative procedures like preconditioned conjugate gradient iterative algorithms can not be used. Consequently, to solve the algebraic problem associated with the global nonconforming procedure (37), we will employ the iterative domain decomposition procedure described below.

Remark: In addition to the low numerical dispersion properties of the space \mathcal{NC}^h , one of the main advantages of using nonconforming elements to solve wave propagation phenomena in parallel architectures is that the amount of information exchanged in a domain decomposition iterative procedure is reduced by half as compared to the case when conforming elements are employed. Consider the decomposed problem over Ω_j satisfying equation (33) in Ω_j , the boundary condition

$$-\sigma[u_j(x, \omega)] \cdot \nu = i\omega\sqrt{\rho}D^{1/2}u_j(x, \omega), \quad x \in \Gamma_j,$$

and the interface consistency conditions

$$\sigma_{jk}\nu_{jk} + i\beta_{jk}u_j = -\sigma_{kj}\nu_{kj} + i\beta_{jk}u_k, \quad x \in \Gamma_{jk} \subset \partial\Omega_j,$$

$$\sigma_{kj}\nu_{kj} + i\beta_{jk}u_k = -\sigma_{jk}\nu_{jk} + i\beta_{jk}u_j, \quad x \in \Gamma_{kj} \subset \partial\Omega_k,$$

where β_{jk} are the components of a positive definite matrix function defined on the interior boundaries Γ_{jk} . The iteration matrix β_{jk} , defined on the interior interfaces Γ_{jk} can be taken to be of the same form as the matrix D in (35) using averaged properties of the coefficients defining D on the adjacent elements Ω_j and Ω_k . Since the objective of the domain decomposition technique is to localize the calculations, we define the iterative procedure at the differential level in the following manner: Find $u_j^n \in [H^1(\Omega_j)]^2$ such that

$$\begin{aligned} &(-\rho\omega^2 u_j^n, \varphi)_j + \sum_j \sum_{pq} (\sigma_{pq}(u_j^n), \varepsilon_{pq}(\varphi))_j + \langle i\omega\sqrt{\rho}D^{1/2}u_j^n, \varphi \rangle_{\Gamma_j} \\ &+ \sum_k \langle [\sigma(u_k^{n-1})\nu_{jk} + i\beta_{jk}(u_j^n - u_k^{n-1})], \varphi \rangle_{\Gamma_{jk}} = (f, \varphi)_j, \quad \varphi \in [H^1(\Omega_{jk})]^2. \end{aligned} \tag{38}$$

To define a discrete iterative procedure we introduce a set Λ^h of Lagrange multipliers λ_{jk}^h associated with the stress values $-\sigma(u_j)\nu_{jk}(\xi_{jk})$:

$$\Lambda^h = \{\lambda^h : \lambda^h|_{\Gamma_{jk}} = \lambda_{jk}^h \in [P_0(\Gamma_{jk})]^2 = [\Lambda_{jk}^h]^2\};$$

here, $P_0(\Gamma_{jk})$ are constant functions on Γ_{jk} .

Motivated by (38), we define the following discrete domain decomposition (hybridized) iterative algorithm:

- (1) Choose an initial guess $(u_j^{h,0}, \lambda_{jk}^{h,0}, \lambda_{kj}^{h,0}) \in \mathcal{NC}_j^h \times [\Lambda_{jk}^h]^2 \times [\Lambda_{kj}^h]^2$.

(2) For all $\{jk\}$, compute $(u_j^{h,n}, \lambda_{jk}^{h,n} \in NC_j^h \times \Lambda_{jk}^h)$ as the solution of the equations

$$\begin{aligned}
 & -(\rho\omega^2 u_j^{h,n}, \varphi)_{jk} + \sum_{pq} (\sigma_{pq}(u_j^{h,n}), \varepsilon_{pq}(\varphi))_{jk} + i\omega \left\langle \left\langle \sqrt{\rho} D^{1/2} u_j^{h,n}, \varphi \right\rangle \right\rangle_{\Gamma_j} \\
 & + \sum_k \left\langle \left\langle \lambda_{jk}^{h,n}, \varphi \right\rangle \right\rangle_{\Gamma_{jk}} = (f, \varphi)_j, \quad \varphi \in NC_j^h
 \end{aligned} \tag{39}$$

and

$$\lambda_{jk}^{h,n} = -\lambda_{kj}^{h,n-1} + i\beta_{jk}[u_j^{h,n}(\xi_{jk}) - u_k^{h,n-1}(\xi_{jk})], \quad \text{on } \Gamma_{jk}. \tag{40}$$

In (39) $\langle \langle \cdot, \cdot \rangle \rangle_{\Gamma_{jk}}$ denote the approximation to the (complex) inner product $\langle \cdot, \cdot \rangle_{\Gamma_{jk}}$ in $L^2(\Gamma_{jk})$ computed using the mid-point quadrature rule. More precisely,

$$\langle \langle u, v \rangle \rangle_{\Gamma_{jk}} = (uv^*)(\xi_{jk})|\Gamma_{jk}|, \tag{41}$$

where $|\Gamma_{jk}|$ is the surface measure of Γ_{jk} . A similar definition holds for $\langle \langle \cdot, \cdot \rangle \rangle_{\Gamma_j}$, changing in (41) ξ_{jk} and Γ_{jk} by ξ_j and Γ_j , respectively.

The argument given in Ha et al. (2002) for isotropic viscoelastic solids can be applied here with minor modifications to show that

$$[u^{h,n} - u^h] \rightarrow 0 \quad \text{in } [L^2(\Omega)]^2 \quad \text{if } n \rightarrow \infty,$$

so that in the limit the global nonconforming Galerkin approximation u^h of (37) is obtained.

6 NUMERICAL RESULTS

The procedure described in the previous section is applied in order to model a seismic experiment called AVO (Amplitude versus Offset). In this technique, it is considered the dependency of the amplitud with the distance between the source and the receiver (offset).

The subsurface is represented by a thin HTI layer embedded between two isotropic media. The P-wave velocity is 2230 m/s for the top layer and 3215 m/s for the layer deeper. The anisotropic material is at a depth of 1 km and its thickness is 100 m. To analyze the type of fluid that fills the fractures, the first experiment takes into account brine-filled fractures, being the vertical P-wave velocity 3905 m/s and the horizontal P-wave velocity 2570 m/s. In the second experiment, gas-filled fractures are considered and the vertical and horizontal P-wave velocity are 3678 m/s and 1895 m/s, respectively.

The 2D domain is a square which side measures 1500 m. We use 300x300 elements. The source is a Ricker wavelet whose principal frequency is 30 Hz and the solution is computed for 160 frequencies in the range of interest from 0 to 80 Hz. The source and the receivers are located at the surface, where 24 receivers are equally distributed between a minimum offset of 250 m and a maximum offset of 1350 m.

The real part of the stiffness coefficients computed were, in the brine case:

$$\begin{pmatrix} 28.15 & 5.33 & 5.33 & 0 & 0 & 0 \\ 5.33 & 12.2 & 5.33 & 0 & 0 & 0 \\ 5.33 & 5.33 & 12.2 & 0 & 0 & 0 \\ 0 & 0 & 0 & 2.87 & 0 & 0 \\ 0 & 0 & 0 & 0 & 2.87 & 0 \\ 0 & 0 & 0 & 0 & 0 & 2.87 \end{pmatrix}, \tag{42}$$

and, in the gas case:

$$\begin{pmatrix} 24.34 & 0.66 & 0.66 & 0 & 0 & 0 \\ 0.66 & 6.45 & 0.66 & 0 & 0 & 0 \\ 0.66 & 0.66 & 6.45 & 0 & 0 & 0 \\ 0 & 0 & 0 & 2.87 & 0 & 0 \\ 0 & 0 & 0 & 0 & 2.87 & 0 \\ 0 & 0 & 0 & 0 & 0 & 2.87 \end{pmatrix} \quad (43)$$

whose values are expressed in GPa.

The synthetic seismograms representing the vertical velocity field of the P-wave are shown below (see Fig. 2 and Fig. 3). The horizontal and vertical axis indicate offset and reflection time, respectively. It can be observed that the amplitudes of the traces are different for both experiments. The case of gas-filled fractures presents large reflectivities at all offsets for the base of the anisotropic layer. Therefore, the numerical results are consistent with the real seismic data.

7 CONCLUSIONS

In first place, this work has a considerable importance in computational poroelasticity, particularly in the use of Finite Element Method to solve Biot's equations.

In this study we present a detailed description of the variational formulation of FEM equations, applied to Biot's equations. We also introduce a brief review of concepts related with anisotropy phenomenon.

We have used a set of numerical quasi-static harmonic experiments to determine the complex and frequency dependent stiffnesses of a viscoelastic transversely isotropic homogeneous medium equivalent to a fluid-saturated poroelastic material containing a dense set of planar fractures. The numerical simulators are based on the finite-element solution of Biot's equations in the diffusive range with boundary conditions representing compressibility and shear tests. The fractures are modeled as very thin highly permeable poroelastic layers of small frame moduli.

The numerical experiments consider brine-filled fractures and gas-filled fractures, representing two different cases.

As a result of these experiments, the stiffness coefficients of the medium were obtained. By performing appropriate rotations in the coordinate system, the VTI medium was converted into an HTI medium as well as the stiffness coefficients.

Finally, the new stiffness matrix was used to build synthetic seismograms. The modeling methodology is based on a finite-element solution of the equations of motion in the space-frequency domain.

The numerical results obtained are consistent with observations in real seismic data. The theory and numerical solver proposed in this work can be applied to more complex geological situations (lower symmetries, stochastic heterogeneities, etc.) and implemented in the processing and interpretation of real seismic data for characterization purposes.

ACKNOWLEDGMENT

This work was partially supported by FONARSEC, CAPP-Ondas, FSTICS06/10, Agencia de Promocion Cientifica y Tecnologica.

REFERENCES

- Carcione J., Picotti S., Gei D., and Rossi G. *Physics and seismic modeling for monitoring CO₂ storage*, volume 163. Pure and Applied Geophysics, 2006.
- Carcione J.M. *Anisotropic Q and velocity dispersion of finely layered media*, volume I. Geophys. Prosp., 1992.
- Carcione J.M. *Wave fields in real media: wave propagation in anisotropic, anelastic, porous and electromagnetic media*, in *Handbook of Geophysical Exploration*, volume 38. Helbig, K. & Treitel, S., Elsevier, Oxford, 2007.
- Carcione J.M., Santos J.E., and Picotti S. *Anisotropic poroelasticity and wave-induced fluid flow. Harmonic finite-element simulation*, volume I. Geophys. J. Internat, 2011.
- Douglas J., Pereira F., and Santos J. *A parallelizable approach to the simulation of waves in dispersive media*, volume 247. Center for Applied Mathematics, Purdue University., 1995.
- Douglas J., Santos J., and Sheen D. *Approximation of scalar waves in the space-frequency domain. Mathematical Models and Methods in Applied Sciences*. 1994.
- Gelinsky S. and Shapiro S. *Poroelastic Backus-averaging for anisotropic, layered fluid and gas saturated sediments*, volume I. Geophysics, 1997.
- Ha T., Santos J.E., and Sheen D. *Nonconforming finite element methods for the simulation of waves in viscoelastic solids*, *Computer Methods in Applied Mechanics and Engineering*. 2002.
- Krief M., Garat J., Stellingwerff J., and Ventre J. *A petrophysical interpretation using the velocities of P and S waves (full waveform sonic)*, volume I. The Log Analyst, 1990.
- Krzikalla F. and Müller T. *Anisotropic P-SV-wave dispersion and attenuation due to interlayer flow in thinly layered porous rocks*, volume I. Geophysics, 2011.
- Love A.M. *A treatise on the mathematical theory of elasticity*, volume I. Dover Publications Inc., 1994.
- Lovera O. and Santos J. *Numerical methods for a model for wave propagation in composite anisotropic media. Mathematical Modelling and Numerical Analysis*. 1988.
- Raviart P.A. and Thomas J.M. *Mixed finite element method for 2nd order elliptic problems*, *Mathematical Aspects of the Finite Element Methods, Lecture Notes of Mathematics*, volume 606. Springer, 1975.
- Santos J.E., Rubino J.G., and Ravazzoli C.L. *A numerical upscaling procedure to estimate effective bulk and shear moduli in heterogeneous fluid-saturated porous media*, volume 198. Comput. Methods Appl. Mech. Engrg, 2009.
- White J.E., Mikhaylova N.G., and Lyakhovitskiy F.M. Low-frequency seismic waves in fluid-saturated layered rocks. *Izvestija Academy of Siences USSR, Physics of Solid Earth*, 10:654–659, 1975.
- Zyserman F., Gauzellino P., and Santos J. *Dispersion analysis of a nonconforming finite element method for the Helmholtz and elastodynamic equations*, volume 58. Int. J. Num. Methods in Engineering, 2003.

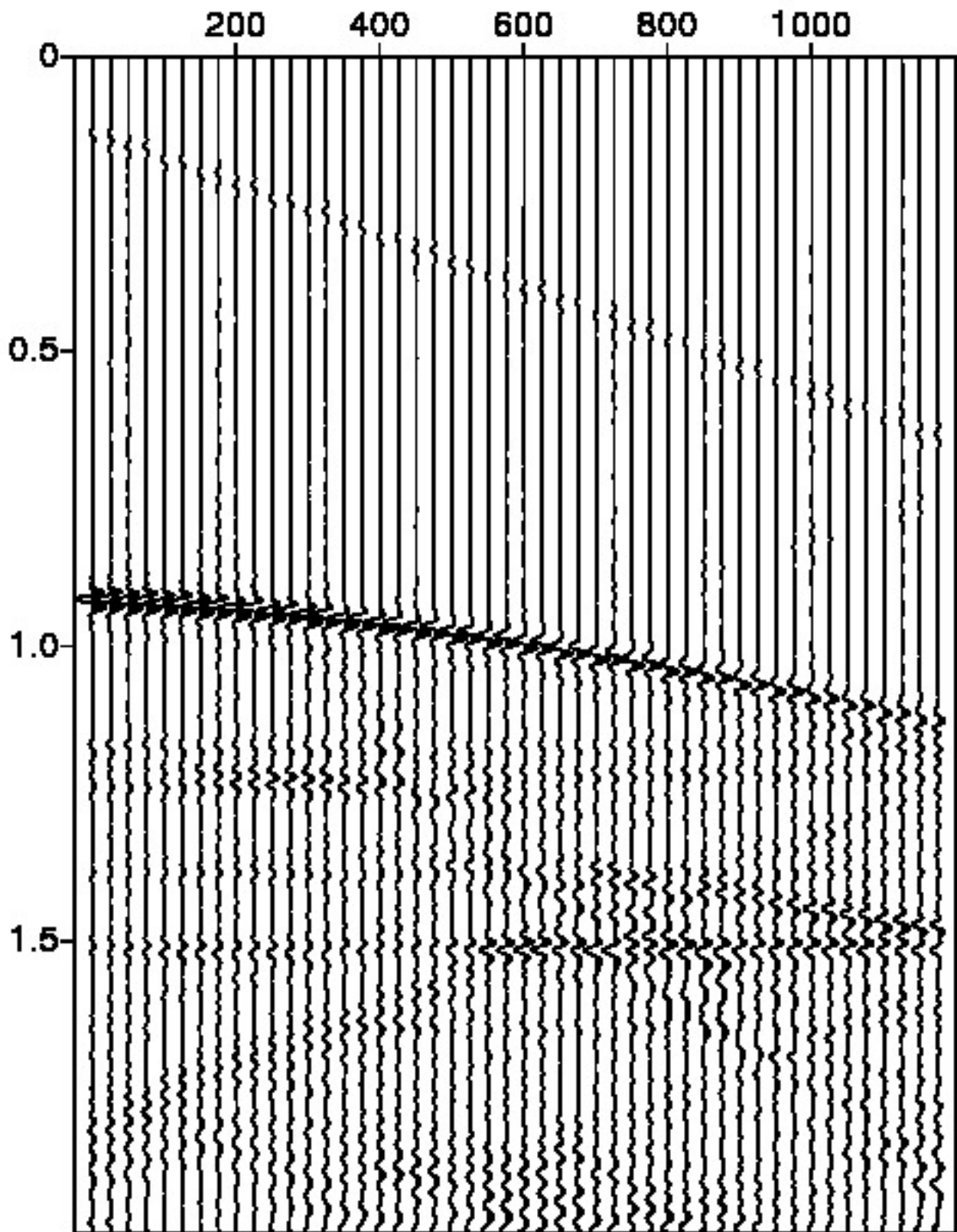


Figure 2: The vertical velocity field of the P-wave for an anisotropic layer with brine saturated fractures.

